Submitted to 1997 IEEE International Conference on Robotics and Automation

Non-Contact Impedance Control for Manipulators Using Visual Information

Toshio Tsuji, Hiromasa Akamatsu and Makoto Kaneko

Computer Science and Systems Engineering
Hiroshima University
Higashi-Hiroshima 739, JAPAN
E-Mail : tsuji@huis.hiroshima-u.ac.jp

Abstract

Impedance control is one of the most effective control method for a manipulator in contact with its environment. In this method, however, the manipulator does not move until an external force is exerted. The present paper proposes a non-contact impedance control which can regulate a virtual impedance between an arm and an external object using visual information. Validity of the proposed method is verified through experiments using a direct-drive robot.

Key Words: Impedance control, robot manipulator, vision-based control, obstacle avoidance

1 Introduction

Impedance control is a method to regulate a mechanical impedance of an end-effector of a manipulator in a desired value according to a given task. It can specify desirable response of the end-effector for an external force before contact. Hogan [1] invented a method to control the end-effector impedance of a manipulator based on measured position, velocity and force of the end-effector using the concept of the resolved acceleration control [2]. Then many studies such as a realization technique without use of an inverse of a Jacobian matrix [3] or without use of a force sensor [4], stability analysis for contact [5], model matching design of the impedance parameter [6] have been conducted. The impedance control is one of the most important framework to control the interaction between the manipulators and the environment.

In some cases, however, occurance of the interaction force between the manipulator and the environment should be carefully considered. For example, when the end-effector handles a fragile object, an approaching velocity of the end-effector should decrease before coming in contact with the object in order to prevent a large impact force. Also in some environments including obstacles, the interaction force between the obstacle and the robot should be avoided. Under the conventional impedance control, it is difficult to cope effectively with such situations, since any external force is not exerted until the end-effector contacts with the objects.

On the other hand, robot motion using vision-based control has been actively studied in recent years [7, 8, 9], where the robot can be controlled according to visual information on the environment. Based on the framework of the vision-based control, Castano and Hutchinson [10] proposed a concept of a visual compliance. This method can constrain the end-effector motion on a virtual task plane based on a hybrid control using the visual sensor information from a camera system and the internal angular sensor information from an encoder at each joint of the manipulator. However, it does not control impedance characteristics itself based on visual information.

Nakabo et al. [11] proposed a concept of a visual impedance and showed that the movement of the end-effector can be modified in real time (remarkably, less than 1 ms sampling time) by using the visual impedance between the end-effector and the object.

We also proposed a vision-based impedance control [12] using a concept of a virtual impedance which was originally proposed for motion planing of a mobile robot [13]. The method can control a virtual impedance between the end-effector and the object as well as the end-effector's impedance. The relative end-effector motion to the object can be controlled without contact through a virtual external force generated by the virtual impedance and visual sensor information.

In this paper, we apply the vision-based impedance control to a redundant manipulator and propose a non-contact impedance control which can utilize kinematic redundancy. The proposed method can control the virtual impedance between the object and multiple points set on the arm including the end-effector, so that the virtual interaction between the whole arm and the environment can be considered.

This paper is organized as follows: in Section II, the impedance control of a manipulator is briefly explained with emphasis on utilization of redundant joint degrees of freedom. Then, the non-contact impedance control is formulated for a redundant manipulator in section III. In section IV and V, computer simulation and experiments are performed in order to clear the distinctive feature of the proposed method.

2 Impedance Control

In general, a motion equation of an m-joint manipulator can be expressed as follows:

$$M(\theta)\ddot{\theta} + h(\theta, \dot{\theta}) = \tau + J^T(\theta)F_{ext}, \quad (1)$$

where $F_{ext} \in \Re^l$ is the external force exerted on the end-effector; $\theta \in \Re^m$ is the joint angle vector; $M(\theta) \in \Re^{m \times m}$is the non-singular inertia matrix (hereafter denoted by M); $h(\theta, \dot{\theta}) \in \Re^m$ is the nonlinear term including the joint torque due to the centrifugal, Coriolis, gravity and friction forces; $\tau \in \Re^m$ is the joint torque vector; $J(\theta) \in \Re^{l \times m}$ is the Jacobian matrix (hereafter denoted by J); and l is the dimension of the task space. For a redundant manipulator, m is larger than l.

Now, the desired impedance of the end-effector is described by

$$M_e d\ddot{X} + B_e d\dot{X} + K_e dX = F_{ext}, \quad (2)$$

where $M_e, B_e, K_e \in \Re^{l \times l}$ are the desired inertia, viscosity and stiffness matrices of the end-effector, respectively; and $dX = X - X_d \in \Re^l$ is the displacement vector between the current end-effector position X and the desired one (namely, the equilibrium position of the end-effector) X_d.

In this paper, we adopt the impedance control law without calculation of the inverse Jacobian matrix presented in [3]:

$$\tau = \tau_{effector} + \tau_{comp}, \quad (3)$$

$$\tau_{effector} = -J^T[M_x(\theta)\{M_e^{-1}(K_e dX + B_e d\dot{x} + \dot{J}\dot{\theta} - \ddot{X}_d\} + \{I - M_x(\theta)M_e^{-1}\}F_{ext}], \quad (4)$$

$$\tau_{comp} = (\bar{J}J)^T\hat{h}(\theta, \dot{\theta}), \quad (5)$$

where $M_x(\theta) = (J\hat{M}^{-1}J^T)^{-1} \in \Re^{l \times l}$ is the operational space kinetic energy matrix [15, 16]; $\bar{J} = \hat{M}^{-1}J^T M_x(\theta) \in \Re^{m \times l}$ is the generalized inverse of J weighted by $\hat{M}^{-1}$; $\tau_{effector} \in \Re^m$ is the joint torque vector needed to produce the desired end-effector impedance; I is the $l \times l$ unit matrix; $\tau_{comp} \in \Re^m$ is the joint torque vector for nonlinear compensation; and $\hat{h}(\theta, \dot{\theta})$, $\hat{M}$ are the estimated values of $h(\theta, \dot{\theta})$ and M. It is assumed that $\hat{h}(\theta, \dot{\theta}) = h(\theta, \dot{\theta})$, $\hat{M} = M$, and the joint configuration θ is not in a singular posture.

Although the control law (3)–(5) or other impedance control methods such as [1], [4] can be applied for controlling redundant manipulators, they cannot effectively utilize arm redundancy. In order to exploit arm redundancy, an additional controller for a subtask can be incorporated into the end-effector impedance control system in parallel [14]:

$$\tau = \tau_{effector} + \tau_{comp} + \tau_{joint}, \quad (6)$$

$$\tau_{joint} = -\Gamma\left(M_j d\ddot{\theta} + B_j d\dot{\theta} + K_j d\theta\right), \quad (7)$$

where $\tau_{joint} \in \Re^m$ is the additional joint control torque for controlling the joint impedance; $M_j, B_j, K_j \in \Re^{m \times m}$ are the desired joint inertia, viscosity and stiffness, respectively; and $d\theta = \theta - \theta_d \in \Re^m$ is the deviation vector between the joint angle θ and the equilibrium joint angle θ_d. Also, the matrix $\Gamma \in \Re^{m \times m}$ can filter out the joint torque in such a way that the filtered joint torque has no effect to the end-effector motion [15, 16]:

$$\Gamma = I - \bar{J}(\bar{J})^+, \quad (8)$$

where $(\bar{J})^+$ denotes the pseudoinverse of $\bar{J}$. It can be easily shown that the additional joint control torque τ_{joint} satisfies the following condition:

$$\bar{J}^T\tau_{joint} = 0, \quad (9)$$

so that τ_{joint} has no dynamic effect to the end-effector motion of the manipulator, and the end-effector impedance remains to be the desired one given by (2).

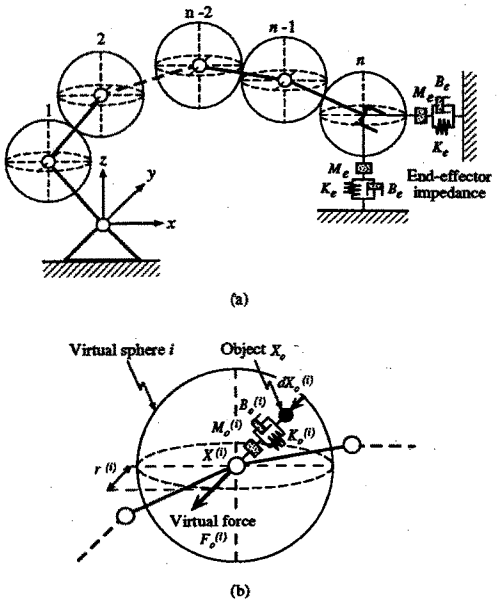

Figure 1: Schematic representation of a Non-Contact Impedance Control (NCIC)

3 Non-Contact Impedance Control

Figure 1 shows a schematic representation of the non-contact impedance control. Let us consider the case that an object approaches a manipulator. In order to consider the interaction between the whole arm and the object without contact, a number of virtual spheres with radius $r^{(i)}(i = 1, 2, \cdots, n)$ are used, where each center of the sphere is located on a link or a joint of the manipulator as shown in Fig. 1 (a). Then, when the object comes into the interior of the virtual sphere i, the normal vector from the surface of the sphere to the object is given as

$$dX_o^{(i)} = X_r^{(i)} - r^{(i)}a^{(i)}, \quad (10)$$

where $X_r^{(i)} = X_o - X^{(i)}$ is the displacement vector from the center of the sphere $X^{(i)} \in \Re^l$ to the object $X_o \in \Re^l$. Also the vector $a^{(i)} \in \Re^l$ is defined as

$$a^{(i)} = \begin{cases} \frac{X_r^{(i)}}{|X_r^{(i)}|} & \left(|X_r^{(i)}| \neq 0\right) \\ 0 & \left(|X_r^{(i)}| = 0\right) \end{cases}, \quad (11)$$

where $|X_r^{(i)}|$ denotes the Euclidian norm of $X_r^{(i)}$. When the object is in the virtual sphere, $|X_r^{(i)}|$ is less than $r^{(i)}$.

Then the virtual non-contact impedance is considered between the object and the center of the virtual sphere as shown in Fig. 1 (b), where $M_o^{(i)}, B_o^{(i)}$ and $K_o^{(i)}$ represent the virtual inertia, viscosity and stiffness matrices associated with the i-th virtual sphere, respectively. Using the non-contact impedance and the displacement vector $dX_o^{(i)}$, the virtual external force $F_o^{(i)} \in \Re^l$ exerted from the object to the center of the sphere is defined as

$$F_o^{(i)} = \begin{cases} M_o^{(i)} d\ddot{X}_o^{(i)} + B_o^{(i)} d\dot{X}_o^{(i)} + K_o^{(i)} dX_o^{(i)} \\ \qquad\qquad \left(|X_r^{(i)}| < r^{(i)}\right) \\ 0 \qquad\qquad \left(|X_r^{(i)}| \geq r^{(i)}\right) \end{cases}. \quad (12)$$

It can be readily seen from (11) and (12) that $F_o^{(i)}$ becomes zero when the object is not in the virtual sphere or the object exists at the center of the sphere.

The virtual external force defined above can be transformed to the equivalent joint torque $\tau_o^{(i)}$:

$$\tau_o^{(i)} = J^{(i)\mathrm{T}} F_o^{(i)}, \quad (13)$$

where $J^{(i)}$ denotes the Jacobian matrix associated with the center of the i-th virtual sphere. For the virtual sphere n defined at the end-effector, the virtual external force $F_o^{(n)}$ is directly incorporated in the motion equation of the end-effector (2):

$$M_e d\ddot{X} + B_e d\dot{X} + K_e dX = F_{ext} + F_o^{(n)}. \quad (14)$$

Consequently, by revising (6) the non-contact impedance control law is given as

$$\tau = \tau_{effector} + \tau_{comp} + \tau_{joint} + \tau_o^{(n)} + \{(1-\alpha) I + \alpha \Gamma\} \sum_{i=1}^{n-1} \tau_o^{(i)}, \quad (15)$$

where α is the parameter which can adjust the relationship between the end-effector motion and the effect of the non-contact impedance. When $\alpha = 1$, $F_o^{(i)} (i = 1, 2, \cdots, n-1)$ does not affect the end-effector motion. On the other hand, when $\alpha = 0$, the end-effector motion is changed by the virtual external force applied to the manipulator except for the end-effector. In addition to the end-effector impedance

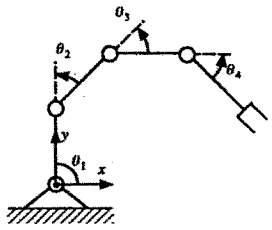

Figure 2: A four-joint planar manipulator

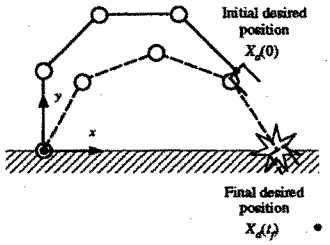

Figure 3: An example of a contact task

control that can regulate M_e, B_e, K_e according to the given task, the relative motion between the manipulator and its environment can be considered through the virtual impedance $M_o^{(i)}, B_o^{(i)}, K_o^{(i)}$ using the non-contact impedance control.

4 Computer Simulation

Computer simulation using a four-joint planar manipulator shown in Fig. 2 was carried out. The parameters of each link of the manipulator are as follows: the length is 0.4 m, the mass 3.75 kg, the moment of inertia 0.8 kgm^2, and the center of mass of each link is at its middle point. The end-effector impedance of the manipulator is determined as M_e = diag.[1, 1] kg, B_e = diag.[20, 20] Nm/s, K_e = diag.[100, 100] N/m, and the desired end-effector position, i.e. the equilibrium position, is simply chosen as its initial position, where the initial posture of the manipulator is $\theta(0) = [\frac{\pi}{2}, -\frac{\pi}{4}, -\frac{\pi}{4}, -\frac{\pi}{4}]^T$ rad.

4.1 Application to contact task

Let us consider a case where the manipulator collides with the environment during movement (Fig. 3). By using the conventional impedance control only, an impact force may arise [17]. Therefore, the non-contact impedance between the end-effector and its environment is used to reduce the impact force.

At first, the characteristics of the environment are represented using an impedance model as follows:

$$M_w \ddot{X} + B_w \dot{X} + K_w (X_s - X) = F_{ext}, \quad (16)$$

where X_s represents the equilibrium position of the environment; and M_w, B_w, K_w are the inertia, viscosity and stiffness of the environment, respectively. Note that $F_{ext} = 0$ when the end-effector is not in contact with the object. In this simulation, M_w = diag.[0, 0.5]

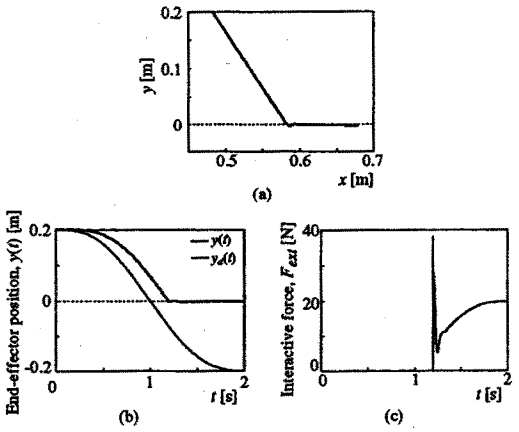

Figure 4: A simulation result of the contact task under the conventional impedance control

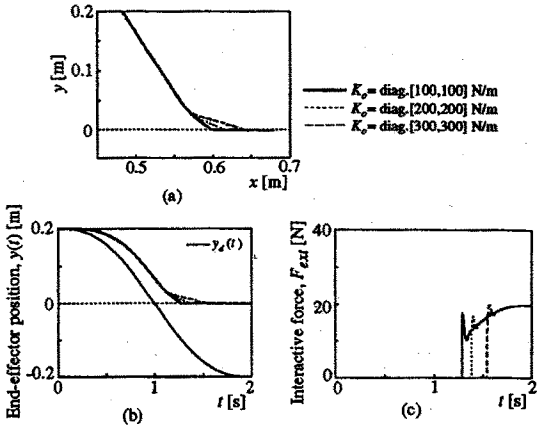

Figure 5: Simulation results of the contact task under the NCIC. Three different virtual stiffness matrices are used.

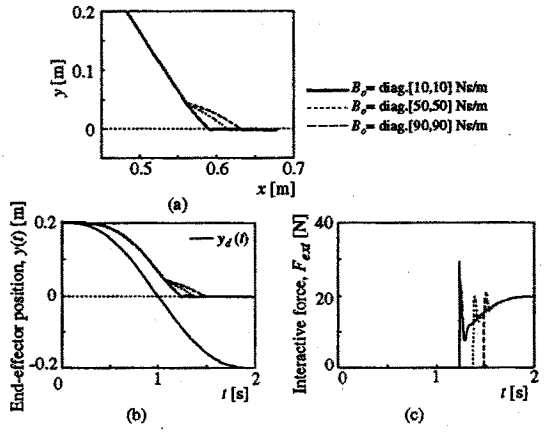

Figure 6: Simulation results of the contact task under the NCIC. Three different virtual viscosity matrices are used.

kg, B_w = diag.[0, 100] Ns/m, K_w = diag.[0, 10000] N/m are used, and the surface of the object is located along the x axis (Fig. 3).

First, Fig.4 represents the simulation result of the contact task under the conventional impedance control, where the end-effector trajectory $X(t)$ in the x–y plane and the time histories of the end-effector trajectory $y(t)$ and the interaction force $F_{ext}(t)$ in the y direction are shown. The desired trajectory $X_d(t)$ of the end-effector is determined using the fifth-order polynomial under the boundary conditions,

$$
\begin{aligned}
X_d(0) &= \left(\frac{1+\sqrt{2}}{5}, 0.2\right) \text{m}, \\
X_d(t_f) &= \left(\frac{2+\sqrt{2}}{5}, -0.2\right) \text{m}, \\
\dot{X}_d(0) &= 0.0\,\text{m/s}, \\
\dot{X}_d(t_f) &= (0,0)\,\text{m/s}, \\
\ddot{X}_d(0) &= (0,0)\,\text{m/s}^2, \\
\ddot{X}_d(t_f) &= (0,0)\,\text{m/s}^2
\end{aligned}
$$

where t_f = 2 s. The computation of the manipulator dynamics was performed by using the Appel's method [18], and the sampling time is 1 ms.

On the other hand, Fig. 5 and 6 show the results under the non-contact impedance control. The virtual circle with its radius $r^{(1)}$ = 0.3 m is used only for the end-effector (n = 1), and the representative point X_o is set on the surface of the object in such a way that X_o is always a normal vector, i. e. the closest, to the surface. In Fig.5, the virtual stiffness $K_o^{(1)}$ are changed as $K_o^{(1)}$ = diag.[100, 100], diag.[200, 200], diag.[300, 300] N/m, whereas constant inertia and viscosity $M_o^{(1)}$ = diag.[0.5, 0.5] kg and $B_o^{(1)}$ = diag.[10, 10] Ns/m are used. Also in Fig.6, the virtual viscosity is changed as $B_o^{(1)}$ = diag.[10, 10], diag.[50, 50], diag.[90, 90] Ns/m with constant inertia and stiffness $M_o^{(1)}$ = diag.[0.5, 0.5] kg and $K_o^{(1)}$ = diag.[0, 0] N/m.

In Fig. 4, large impact force is observed when the end-effector collides with the object. On the contrary, in Fig. 5 and Fig. 6, the end-effector slows down before contact, so that the impact force decreases considerably. It can be seen that the virtual external force acts to the end-effector in the direction for avoiding the collision with the object.

4.2 Application to object avoidance

Next, let us consider the manipulator close to the object. By using the conventional impedance control only, the manipulator cannot take any action for avoiding the object without the interaction force.

As the first example of the non-contact impedance control, virtual circle is attached at the end-effector (n = 1) as shown in Fig. 7. The time histories of the end-effector trajectory $x(t)$ and the object trajectory

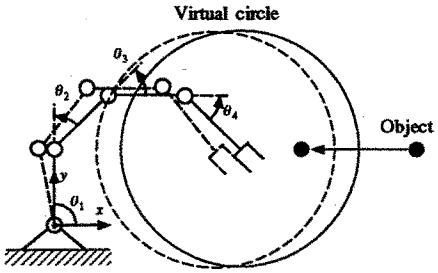

Figure 7: Avoidance of an object using the NCIC

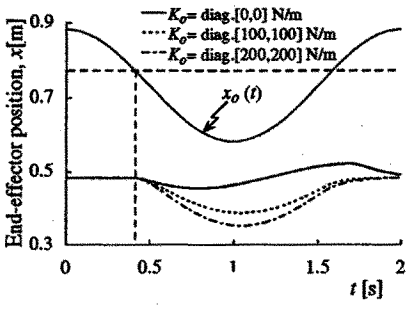

Figure 8: Change of the end-effector trajectories for the object under the NCIC

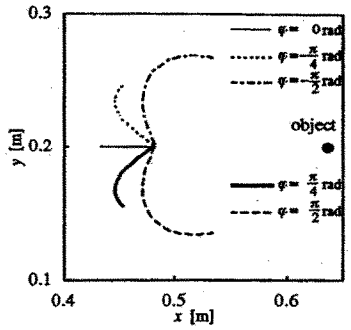

Figure 9: Control of the end-effector trajectories via the non-contact impedance matrices

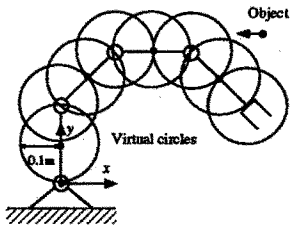

Figure 10: A manipulator and virtual circles

$x_o(t)$ in the x direction are shown in Fig. 8, where the radius of the sphere is $r^{(1)} = 0.3$ m; and the virtual stiffness is changed as $K_o^{(1)} = \text{diag.}[0, 0]$, diag.[100, 100], diag.[200, 200] N/m with constant inertia and viscosity $M_o^{(1)} = \text{diag.}[0.5, 0.5]$ kg, $B_o^{(1)} = \text{diag.}[10,10]$ Ns/m. The object is oscillating with the period of 2 s and the amplitude of 0.2 m in the direction of x axis as shown in Fig. 7. When the distance between the end-effector and the object is more than $r^{(1)}$, the end-effector does not move. However, when the object comes into the virtual circle, the end-effector is displaced in the direction opposite to the object. Also the trajectories of the end-effector reflects the stiffness between the end-effector and the object.

Next, the non-contact impedance matrices $M_o^{(1)}$, $B_o^{(1)}$, $K_o^{(1)}$ are changed as

$$\begin{aligned} M_o^{(1)} &= R(\varphi)\ \text{kg}, \\ B_o^{(1)} &= 10R(\varphi)\ \text{Ns/m}, \\ K_o^{(1)} &= 50R(\varphi)\ \text{N/m}, \\ R(\varphi) &= \begin{pmatrix} \cos\varphi & -\sin\varphi \\ \sin\varphi & \cos\varphi \end{pmatrix}, \end{aligned}$$

and the step response of the end-effector is examined, where the object is located at the position with a distance 0.15 m apart from the initial position of the end-effector in the direction of x axis. According to the rotation matrix $R(\varphi)$, the direction of the virtual external force is rotated with the angle φ in the counter-clockwise direction from the direction of the vector $dX_o^{(1)}$.

Figure 9 shows the change of the step responses of the end-effector with the angle φ. The response of the end-effector (namely, the amplitude and the direction) can be controlled by regulating the non-contact impedance matrices.

In the second example of the non-contact impedance control, eight virtual circles are used ($n = 8$) as shown in Fig. 10, where the centers of the circles are located at the middle point of each link and each joint except for the first joint.

Figures 11 and 12 show the change of the arm posture for the moving object. The radius of each circle is $r^{(i)} = 0.1$ m and the virtual impedance are $M_o^{(i)} = \text{diag.}[2, 2]$ kg, $B_o^{(i)} = \text{diag.}[40, 40]$ Ns/m, $K_o^{(i)} = \text{diag.}[200, 200]$ are used. Also the desired joint impedance in (7) are chosen as $M_j = \text{diag.}[0.01, 0.01, 0.01, 0.01]$ kgm^2, $B_j = \text{diag.}[0.2, 0.2, 0.2, 0.2]$ Nm/(rad/s), $K_j = \text{diag.}\ [1, 1, 1, 1]$ N/rad. The parameter α in (15) is $\alpha = 1$ in Fig. 11 so that the arm redundancy is utilized. On the other hand, $\alpha = 0$ in Fig. 12. It can be seen from both the figures that the manipulator moves without contact and the use of the arm redundancy can be specified using the parameter α.

5 Experiments

5.1 Experimental apparatus

The experiment of the non-contact impedance control was carried out using a direct-drive robot (three-

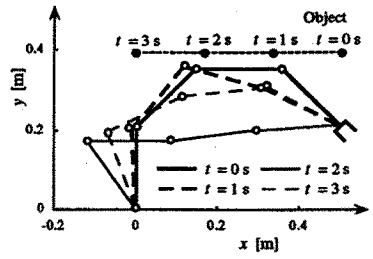

Figure 11: Avoidance of an object using the NCIC ($\alpha = 1$)

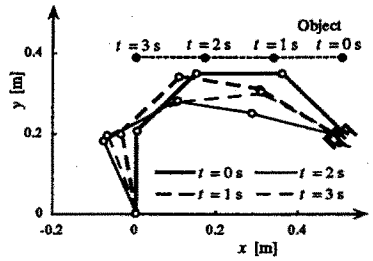

Figure 12: Avoidance of an object using the NCIC ($\alpha = 0$)

joint planar type, KOBELCO) and a PSD camera system to measure the position of the object as shown in Fig.13. Table 1 shows the link parameters of the robot. The task space is the horizontal plane and a LED is attached at a tip of a stick in order to represent the point object, where the measurement error is less than ± 3 mm in the task space. The computation of the control law is performed by using four CPUs (Transputer, T800, 25MHz).

5.2 Robust Impedance Control

The impedance control cannot regulate the end-effector impedance perfectly without an accurate model of the robot dynamics. Also, unexpected external disturbances are often applied to the robot, so that errors between the desired impedance and the realized one may arise. We develop a robust impedance control in the presence of modeling error for the experiments using the direct-drive robot.

The impedance controller is divided into two part as shown in Fig. 14: the impedance filter and the robust position controller.

5.2.1 Impedance filter

This part computes the ideal trajectory of the end-effector X_v from the measured external force F_{ext}, the computed virtual external force$F_o^{(n)}$ and the desired end-effector impedance, which must be satisfied to realize the desired impedance:

$$M_e\ddot{X}_v + B_e\dot{X}_v + K_eX_v = V_d, \tag{17}$$

$$V_d = F_{ext} + F_o^{(n)} + M_e\ddot{X}_v + B_e\dot{X}_v + K_eX_v, \tag{18}$$

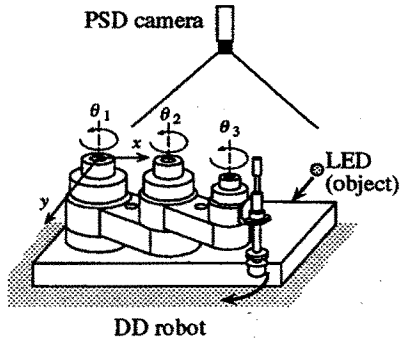

Figure 13: Experimental apparatus

Table 1: Link parameters of the robot

	link 1	link 2	link 3
length (m)	0.25	0.25	0.125
mass (kg)	20.8	13.2	8.84
center of mass (m)	0.064	0.065	0.031
moment of inertia (kgm^2)	0.334	0.196	0.0851
joint friction (Nms/rad)	2.69	1.88	0.0634

where $X_v = [x_v^1, x_v^2, \cdots, x_v^l]^T$; and $V_d = [v_d^1, v_d^2, \cdots, v_d^l]^T \in \Re^l$ is the modified total disturbance force. Since the initial values of X_v, $\dot{X}_v$, $\ddot{X}_v$ are known and the desired end-effector impedance M_e, B_e, K_e and the desired (equilibrium) position X_d, $\dot{X}_d$, $\ddot{X}_d$ are given, X_v can be solved numerically based on F_{ext} and $F_o^{(n)}$.

5.2.2 Robust position controller

Using the ideal trajectory of the end-effector X_v, the state feedback controller is designed. Transforming the motion equation the manipulator into the task space, we have

$$M_x(\theta)\ddot{X} + \mu_x(\theta,\dot{\theta}) = F + F_{ext}, \tag{19}$$

where $\mu_x(\theta,\dot{\theta}) = (M^{-1}(\theta)J^TM_x)^Th(\theta,\dot{\theta}) - M_x\dot{J}\dot{\theta} \in \Re^l$; and $F \in \Re^l$ is the equivalent end-effector force generated by τ. The end-effector control force F is defined as follows:

$$F = \hat{M}(\theta)_x a^* + \hat{\mu}_x(\theta,\dot{\theta}) - F_{ext}, \tag{20}$$

$$a^* = M_e^{-1}V - M_e^{-1}B_e\dot{X} - M_e^{-1}K_eX, \tag{21}$$

where $V = \left[v^1, v^2, \cdots, v^l\right]^T \in \Re^l$ is the input to the feedback controller; and $\hat{M}_x(\theta)$ and $\hat{\mu}_x(\theta,\dot{\theta})$ are the estimated values of $M_x(\theta)$ and $\mu_x(\theta,\dot{\theta})$, respectively. In the presence of the modeling error, $\hat{M}_x(\theta) \neq M_x(\theta)$ and $\hat{\mu}_x \neq \mu_x$. Therefore the error $E_m = \left[E_m^1, E_m^2, \cdots, E_m^l\right]^T \in \Re^l$ arises in the end-effector motion equation by substituting (20), (21) into (19):

$$M_e\ddot{X} + B_e\dot{X} + K_eX = V + E_m. \tag{22}$$

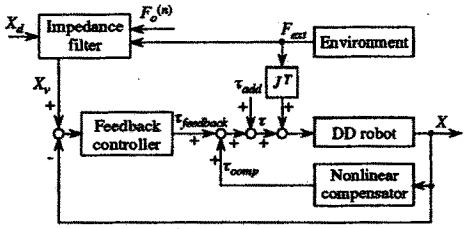

Figure 14: Robust impedance control of a direct-drive robot in the presence of modeling error

Now, let us derive the input V of (22) which results (17). Kuo and Wang [19] proposed the robust position feedback control in the task space based on the following simple model of the error signal E_m:

$$[E_m]^{(p)} = \sum_{j=1}^{p} B_j [E_m]^{(p-j)}, \tag{23}$$

where $[E_m]^{(p)}$ denotes the p-th time derivative of E_m. In this paper, assuming $p = 1$ and $b_1 = 0$ for simplicity, we can derive the following state equation from (17), (22), (23):

$$\dot{Z} = LZ + MS, \tag{24}$$
$$e = NZ, \tag{25}$$

where $Z = [e, \dot{e}, \ddot{e}]^T \in \Re^{3l}$, $S = \dot{E}_m \in \Re^l$, $e = X - X_v$, $E_m = V - V_d$. Also L, M, N are defined as

$$L = \begin{bmatrix} 0 & I & 0 \\ 0 & 0 & I \\ 0 & -M_e^{-1}K_e & -M_e^{-1}B_e \end{bmatrix} \in \Re^{3l \times 3l},$$
$$M = \begin{bmatrix} 0 & 0 & 2M_e^{-1^T} \end{bmatrix}^T \in \Re^{3l \times l},$$
$$N = [I \quad 0 \quad 0] \in \Re^{l \times 3l},$$

where $I \in \Re^{l \times l}$ and $0 \in \Re^{l \times l}$ denote the unit matrix and the zero matrix, respectively.

For the state equation derived above, we apply the state feedback

$$S = -KZ, \tag{26}$$

where $K = [K_1, K_2, K_3] \in \Re^{l \times 3l}$ is the feedback gain matrix which should be chosen in such a way that Z in (24) converges to zero faster than the change of X_v. We can choose the diagonal matrix for $K_i = \text{diag.}\,[k_i^1, k_i^2, \cdots, k_i^l] \in \Re^{l \times l}$ for simplicity. As a result, we have

$$\dot{E}_m = K_1 e + K_2 \dot{e} + K_3 \ddot{e}, \tag{27}$$

so that we can compute the control input V_x.

Consequently the robust impedance control law is given as follows:

$$\tau = \tau_{feedback} + \tau_{comp} + \tau_{add}, \tag{28}$$

$$\tau_{feedback} = J^T(\hat{M}_x(\theta)a^* - F_{ext}, \tag{29}$$

$$\tau_{comp} = J^T \hat{\mu}_x(\theta, \dot{\theta}), \tag{30}$$

$$\tau_{add} = \tau_{joint} + \{(1-\alpha)I + \alpha\Gamma\} \sum_{i=1}^{n-1} \tau_o^{(i)}. \tag{31}$$

Under the above control law, the resulted end-effector trajectory X agrees with the ideal trajectory of the end-effector X_v computed by the impedance filter, so that the desired end-effector impedance can be realized. In the experiments in this paper, the feedback gain $K_i = \text{diag.}[13.5, 5.75, 0.925]$ $(i = 1, 2)$ is used, which results the poles $P_i = [-6, -6, -6]$ $(i = 1, 2)$ of the closed loop (24) and (26).

5.3 Experimental results

The end-effector impedance of the robot is $M_e = \text{diag.}[25, 25]$ kg, $B_e = \text{diag.}[200, 200]$ Ns/m, $K_e = \text{diag.}[400, 400]$ N/m; and the desired end-effector position is chosen as its initial position $X_d = [0.4, 0]^T$ m, where the initial posture is $\theta(0) = [0.8, -1.02, -1.49]^T$ rad.

The virtual circle with its radius $r = 0.3$ m is used only for the end-effector $(n = 1)$, and the step responses of the end-effector are measured, where the object is located at the position with a distance 0.2 m apart from the initial position of the end-effector in the direction of y axis. Figure 15 (a) shows the experimental results of the step responses, where the virtual viscosity $B_o^{(1)}$ is changed as $B_o^{(1)} = \text{diag.}[20, 20]$, diag.[100, 100], diag.[200, 200] Ns/m with constant inertia and stiffness $M_o^{(1)} = \text{diag.}[4, 4]$ kg, $K_o^{(1)} = \text{diag.}[400, 400]$ N/m. Also in Fig. 15 (b) the error $e_y(t)$ between the measured trajectory X and the ideal end-effector trajectory X_v computed from (17),(18) are shown. The sampling time is 2.6 ms. The step response of the end-effector changes depending on $B_o^{(1)}$, and the control error is quite small.

Figure 16 shows the end-effector trajectory $X(t)$ for the moving object $X_o(t)$, where $r^{(1)} = 0.2$ m; $M_o^{(1)} = \text{diag.}[4, 4]$ kg; $B_o^{(1)} = \text{diag.}[80, 80]$ Ns/m; $K_o^{(1)} = \text{diag.}[400, 400]$ N/m. The posture of the robot changes according to the motion of the LED.

6 Conclusion

The present paper proposed the non-contact impedance control that can control the virtual impedance between the manipulator and the environment as well as the end-effector impedance. This method uses the virtual interaction force in order to express the relationship between the manipulator and the environment without contact and the dynamics of the relative motion of the manipulator to the object can be regulated. Also the arm redundancy can be utilized in the framework of the non-contact impedance control. The validity and feasibility were confirmed through the computer simulation and the robot experiments.

This method includes several parameters such as the location and the size of the virtual sphere, the joint and virtual impedance matrices, the parameter

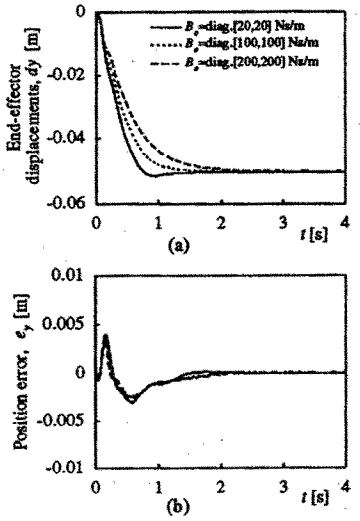

Figure 15: Step responses of the end-effector under the NCIC

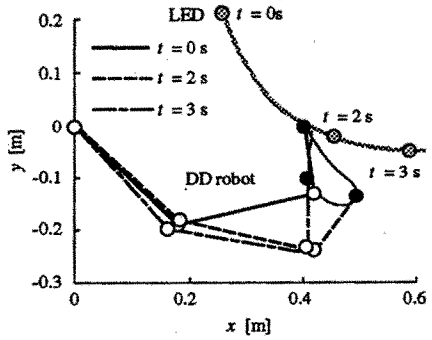

Figure 16: The DD robot avoiding the object

for the use of the arm redundancy. Future research will be directed how the parameters can be determined according to the given task and its environment.

References

[1] N.Hogan, "Impedance Control: An Approach to Manipulation, Parts I, II, III," ASME journal of Dynamic Systems, Measurement, and Control, 107, 1, pp.1–24, 1985.

[2] J. Y. S. Luh, M. W. Walker and R. P. Paul, "Resolved Acceleration Control of Mechanical Manipulators," IEEE Trans. on Automatic Control, AC-25, pp.468–574, 1980.

[3] N. Hogan, "Stable Execution of Contact Tasks Using Impedance Control," Proc. of IEEE International Conference on Robotics and Automation, pp.1047–1054, 1987.

[4] S. Tachi, T. Sakaki, H. Arai, S. Nishizawa and J. F. Pelaez-Polo, "Impedance Control of a Direct-Drive Manipulator without Using Force Sensors," Advanced Robotics, vol.5, no.2, pp.183-205, 1991.

[5] E. Colgate and N. Hogan, "An Analysis of Contact Instability in terms of Passive Physical Equivalents," Proc. of IEEE International Conference on Robotics and Automation, pp.404–409, 1989.

[6] Z. W. Luo and M. Ito, "Control Design of Robot for Compliant Manipulation on Dynamic Environments," IEEE Trans. on Robotics and Automation, Vol. 9, No. 3, pp. 286–296, 1993.

[7] J. E. Agapakis, J. M. Katz, J. M. Friedman and G. N. Epstein, "Vision-aided Robotic Welding: An Approach and a Flexible Implementation," International Journal of Robotics Research, vol.9, no.5, pp.17–33, 1990.

[8] B. Espiau, F. Chaumette and P. Rives, "A new approach to visual servoing in robotics," IEEE Trans. on Robotics and Automation, vol.8, no.3, pp.313–326,1992.

[9] R. Sharma, J. -Y. Herve and P. Cucka, "Dynamic robot Manipulation Using Visual Tracking," in Proc. of IEEE International Conference on Robotics and Automation, vol. pp.1844–1849, 1992.

[10] A. Castano and S. Hutchinson "Visual Compliance: Task-Directed Visual Servo Control," IEEE Trans. on Robotics and Automation, vol.10, no.3, pp.334–342, 1994.

[11] Y. Nakabo, I. Ishii and M. Ishikawa, "Robot Control Using Visual Impedance," Proc. of JSME Annual Conference on Robotics and Mechatronics '96, Vol.B, pp.999–1002, 1996. (In Japanese)

[12] M. Hatagi, H. Akamatsu, T. Tsuji and M. Kaneko, "Non-Contact Impedance Control for Manipulators," Proc. of JSME Annual Conference on Robotics and Mechatronics '96, Vol.B, pp.853–856, 1996.(In Japanese)

[13] T. Arai, H. Ogata and T. Suzuki, "Collision Avoidance Among Multiple Robots Using Virtual Impedance," Proc. of IEEE/RSJ International Workshop on Intelligent Robots and Systems, pp. 479–485, 1989.

[14] T. Tsuji and A. Jazidie, "Impedance Control for Redundant Manipulators: An Approach to Joint Impedance Regulation Utilizing Kinematic Redundancy," Journal of the Robot Society of Japan, Vol. 12, No. 4, pp.1072–1078, 1994. (In Japanese)

[15] O. Khatib, "A Unified approach for motion and force control of robot manipulators: the operational space formulation," IEEE J. of Robotics and Automation, vol.RA-3, no.1, pp.43-53, 1987.

[16] O. Khatib, "Motion/Force Redundancy of Manipulators," Proc. of Japan-U.S.A. Symposium on Flexible Automation, 1, pp.337-342, 1990.

[17] T. Tsuji, K. Ito and P. Morasso," Neural Network Learning of Robot Arm Impedance in Operational Space," IEEE Trans. on Systems, Man and Cybernetics - PartB: Cybernetics, vol.26, No.2, pp.290–298, 1996.

[18] V. Potkonjak and M. Vukobtatovic, "Two New Methods for Computer Forming of Dynamic Equation of Active Mechanisms," Mechanism and Machine Theory, vol.14, no.3, pp.189–200, 1987.

[19] C. Y. Kuo and S. P. T. Wang, "Robust Position Control of Robotic Manipulator in Cartesian Coordinates," IEEE Trans. on Robotics and Automation, vol. 7, no. 5, pp. 653–659, 1991.